Available online at www.sciencedirect.com

ScienceDirect

Advances in Space Research 57 (2016) 543–551

ADVANCES IN SPACE RESEARCH (a COSPAR publication)

www.elsevier.com/locate/asr

An improvement of the sensitivity of GPS radio occultation data to detect gravity waves through observational and modeling factors

P. Alexander [a,*], A. de la Torre [b], R. Hierro [b], P. Llamedo [b]

[a] Instituto de Física de Buenos Aires, CONICET, Ciudad Universitaria Pabellón 1, 1428 Buenos Aires, Argentina
[b] Facultad de Ingeniería, Universidad Austral, Av. J. de Garay 125, 1063 Buenos Aires, Argentina

Received 29 May 2015; received in revised form 30 October 2015; accepted 31 October 2015
Available online 6 November 2015

Abstract

There is a mid-latitude region to the East of the Andes Range in the Southern Hemisphere that exhibits ideal conditions for the generation of gravity waves (GW) by topography mainly during winter. The configuration favors the generation of wavefronts that are parallel to the North–South direction. Global Positioning System (GPS) radio occultation (RO) retrievals from the COSMIC (Constellation Observing System for Meteorology, Ionosphere and Climate) mission exhibit in a large proportion of the soundings an orientation which should be favorable to the detection of these wavefronts. We try to verify if this GW activity surplus on the East with respect to the West in the studied zone in winter emerges clearly in the GPS RO data between years 2007 and 2012. We argue that the orientation of the soundings but also the mathematical model selected to represent the GW energy distribution can affect the possibility of detecting the signatures of the waves. In particular, we explore a new interpretation of the GW energy distribution observed by GPS RO at the lowest values, as they stay below the precision limit of the technique. We suggest to replace that part of the measured distribution by an exponential curve that in general suits the trend of all the other observed energies. In following this alternative it is shown that the calculated mountain wave activity in the studied sector is now even more clearly larger in the East than in the West during winter. Finally, we consider that energy distributions observed with any measurement technique should in general not be considered as the solely contribution from waves, as also other variable phenomena may be adding to the final outcome.

Keywords: Gravity waves; Radio occultation; Energy distribution

1. Introduction

A Global Positioning System (GPS) radio occultation (RO) occurs whenever a transmitting satellite from the global navigation network at an altitude about 20,000 km rises or sets from the standpoint of a low Earth orbit (LEO) receiving satellite at a height of about 800 km and the signal goes across the atmospheric limb (Jin et al., 2011, e.g.,). The Doppler frequency alteration produced through refraction of the ray by the Earth's atmosphere in the trajectory between the transmitter and the receiver is detected and then may be converted into slant profiles of diverse variables in the neutral atmosphere and the ionosphere (Kursinski et al., 1997, e.g.,). GPS RO observations have been used to study gravity waves (GW), mainly in the stratosphere due to the lower reliability of the temperature profiles in the moist portion of the troposphere and the problems of isolating the waves around the tropopause due to its sharp kink. In April 2006 the Constellation Observing System for Meteorology, Ionosphere and Climate (COSMIC) launched six low Earth orbit (LEO) satellites. The mission aimed to produce up to 2500 GPS RO daily with global distribution.

* Corresponding author. Tel.: +54 11 4576 3353; fax: +54 11 4576 3357.
E-mail addresses: peter@df.uba.ar (P. Alexander), adelatorre@austral.edu.ar (A. de la Torre), rhierro@austral.edu.ar (R. Hierro), pllamedo@austral.edu.ar (P. Llamedo).

http://dx.doi.org/10.1016/j.asr.2015.10.047
0273-1177/

We should note the interesting characteristics of the region to be analyzed. In the latitude interval 29–36S, an imaginary line through the highest peaks (some of them above 6000 m), is nearly equivalent to the meridian at the longitude 70 W (see Fig. 1). The zone to the East represents a natural laboratory of GW where several types of sources may be present (de la Torre and Alexander, 2005; de la Torre et al., 2006). On one hand there is a forcing of the GW by the intense prevailing tropospheric westerlies mainly during winter. The orientation of topography leads to the preferential generation of two-dimensional GW with constant phase planes nearly aligned North–South, as suggested by theory (Baines, 1995) and shown by numerical simulations (Llamedo, 2009, e.g.,). These mountain waves (MW) are expected to be quite non-hydrostatic. All other types of waves should not exhibit preferential orientations. Deep convection occurs mainly around summer and could also be a significant source of non-hydrostatic GW. Ideal convective clouds may become isotropic gravity wave sources (Alexander et al., 2009). Also, a westerly tropospheric jet is permanently located around 30S and exhibits an annual variability, so inertio-gravity (IGW) waves could be generated by geostrophic adjustment. Additional sources may be present due to instabilities by vertical shear of wind or the entrance of cold fronts from the South once every week or so.

Due to the spherical assumption implicit in the derivation of neutral atmosphere variables (Kursinski et al., 1997), the aptitude of GPS RO to detect non-hydrostatic GW becomes doubtful. Only modes with horizontal wavelengths of several 100 km should be a priori visible due to the observational filter of this technique (Wu, 2006), mainly IGW. Alexander et al. (2008) have shown that GPS RO has some potential to detect GW with horizontal wavelengths shorter than about 200 km, but it depends on a smearing effect which is ultimately related to the horizontal angle between the line of sight (LOS) of the retrieval and the wavefronts to be detected. If the LOS of a sounding is in every observational point parallel to the horizontal component of the wave vector, only a weak signature, if any, will be detected, because the integrated measure along the LOS will tend to be canceled out by successive positive and negative contributions of the wave. On the other hand, if the LOS is in every observational point contained in a wavefront, then there is no significant smearing along the LOS, as the scanning is performed on a constant phase surface and therefore no successive cancelations will occur. This is an optimal situation which we will try to exploit in the present work. Although the above descriptions apply to each separate mode, the outcome of a sounding in the real atmosphere is the aggregate of a very complex three-dimensional combination of waves and other mesoscale structures. As in general waves may have arbitrary orientations and the background atmosphere may have some significant level of variability or may exhibit the presence of different kind of mesoscale features, it becomes rather problematic to make inferences in single soundings. However, the use of known preferential climatological wave characteristics (like MW with well-known usual orientation) may help us to extract useful information from statistical results and push the filtering window of the method (regarding detectable horizontal wavelengths) into observational ranges a priori considered inaccessible. We will test this idea in the present work in a region which exhibits these favorable characteristics. We evaluate here the sensitivity of the GPS RO retrievals in the neutral atmosphere to detect GW by the use of potential energy as an indicator of activity within the temperature profiles. If the angle between the LOS and the horizontal wave vectors are randomly distributed, (Alexander et al., 2008) showed that for different GW scenarios the observed mean energy for a large number of retrievals could be about 20% smaller than the true one. GW activity (quantified by amplitudes or potential energies) inferred from GPS RO data has been generally found to be smaller than that obtained by other observational methods due to its scan characteristics (only some specific relative orientations between LOS and waves are favorable and in addition the extensive horizontal region sounded by the technique may easily exceed the localization of the waves). In the geographical zone here studied, the wavefronts generated by topography usually exhibit a North–South alignment, which implies that LOS along the same direction will more likely lead to the presence of wave signatures in the measured profiles. In fact, (Alexander et al., 2009) noticed that COSMIC RO have LOS preferentially oriented about the North–South direction. (Baumgaertner and McDonald, 2007; McDonald and Hertzog, 2008) analyzed this effect above the Antarctic Peninsula. This zone and the Southern Andes

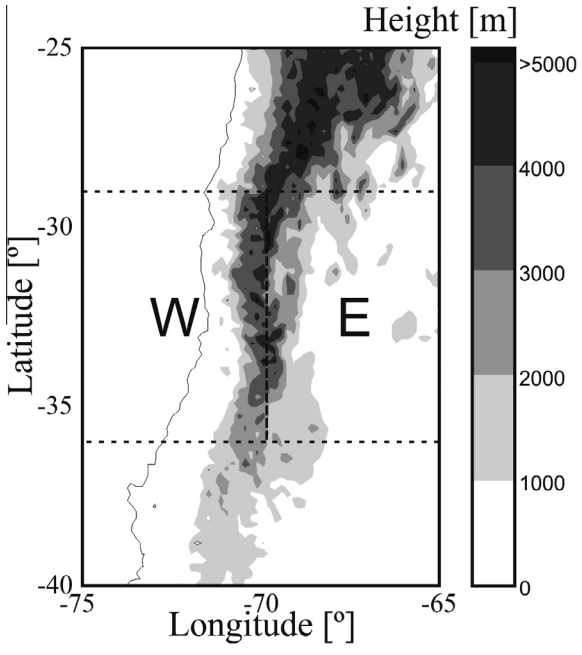

Fig. 1. The region under study and the surroundings to the North and to the South.

are usually considered a stratospheric GW hot spot due to the high activity levels (Hindley et al., 2015, e.g.,).

In addition we wish to address an issue which is often avoided, regarding the interpretation of all fluctuations in vertical profiles of temperatures in a given vertical wavelength range as GW, whereas it has already been mentioned that these are neither omnipresent nor permanent (Alexander and Barnet, 2007). The intermittent characteristic of the GW and the random possibility of GPS RO of having a favorable or adverse observational orientation for their observation gives to the technique a statistical value. Then, the GW energy distribution provided by a significant number of observations will characterize in a statistical way the status of the analyzed region in a given month or season (Llamedo, 2009, e.g.,). The COSMIC mission has significantly increased the amount of available GPS RO since the second half of year 2006.

Sacha et al. (2014) have shown that part of the non-hydrostatic GW spectrum is filtered out or attenuated when using temperature profiles of GPS RO and suggested instead the use of the measured density. As an alternative to this option, the present study may improve the detection of non-hydrostatic GW from temperature observations (after they lost part of their quality due to diverse assumptions in the GPS RO derivation of atmospheric quantities), whereas hydrostatic GW should be much less affected by the retrieval process.

2. Data and processing

We considered 6 complete years (2007–2012) of the GPS RO post-processed data (product version 2010.2640) available at CDAAC (COSMIC Data Analysis and Archive Center) in the rectangle defined by 29–36S and 65–75 W. The latitude interval was selected due to the very high mountains and the nearly perfect alignment of the highest tops with the 70 W meridian (see Fig. 1), so this longitude constitutes the border between two regions we defined in the above rectangle: to the East (E) of the Andes Range (where wavefronts generated by topography with North–South orientation are expected) and to the West (W). We processed 4089 so-called dry temperature profiles to quantify GW activity by potential energy per unit mass E_p in a layer between vertical positions z_1 and z_2 (lower stratosphere) according to the equation (Wilson et al., 1991).

$$E_p = \frac{1}{2}\frac{1}{(z_2 - z_1)}\int_{z_1}^{z_2}\left(\frac{g}{N}\right)^2\left(\frac{T'}{T_b}\right)^2 dz \quad (1)$$

where g and N refer to gravity of Earth and the Brunt-Väisälä frequency, whereas T_b and T' correspond to the background and gravity wave components of the temperature profile T usually separated by the use of a digital filter. Calculations are preformed only in the stratosphere to avoid problems with the digital filter close to the tropopause (Alexander, 2011). The uncertainty in the calculation of E_p depends not only on the accuracy of T, but also on the particular choice of z_1, z_2, the filter itself (diverse types have different response curves) and the cutoffs that determine the separation limits in vertical wavelength between noise, background and waves (Luna et al., 2013). If all the latter disturbing factors are eliminated by using the same scheme in all calculations, then only the uncertainty related to the accuracy of the retrieved T remains, which in a pessimistic scenario propagates into a mean E_p as a standard deviation below 8% (Luna et al., 2013). The lower and upper wavelength filter cutoffs were set to 3 and 12 km to eliminate noise that may be contaminating the profiles (Marquardt and Healy, 2005) and to separate the largest observable waves from the background (de la Torre and Alexander, 2005, e.g.,). The vertical integration column was selected between 19 and 31 km. To determine the lower limit we analyzed the available 4089 profiles, which typically exhibit tropopauses between 15 and 19 km. Tropopause height and temperature are provided by the retrievals according to two usual but different ways: the cold point determination and the lapse rate definition as given by the World Meteorological Organization (WMO). The cold point tropopause is not used here because it is usually considered to be physically meaningful only in the tropics. In about 95% of the cases the WMO tropopause was found below 19 km height. The upper limit of the vertical column was determined at 31 km due to the low reliability of the profiles for GW E_p calculations at higher altitudes (Luna et al., 2013).

We classified the GPS RO profiles according to their location (stratospheric portion of the sounding totally contained in the E or W sector, rejected if there was a mixed presence) and to their LOS: favorable (F) for MW detection if the LOS was contained in the cone determined by $\pm 30°$ with respect to North–South and unfavorable (U) if it was further away than $\pm 45°$, events in between were considered intermediate cases and were therefore discarded. Finally the four resulting groups where separated according to the month of occurrence into the corresponding season in the Southern Hemisphere: summer (DJF), autumn (MAM), winter (JJA), spring (SON). The sector, LOS and season classifications lead to 16 different categories.

Generalizing the above idea, it is usually assumed that the measured profiles of atmospheric variables like temperature, density or wind may be essentially decomposed into two main components: background and waves (Alexander and Barnet, 2007, e.g.,). Space and time variations of the background are much smoother than those pertaining to the waves. John and Kumar (2013) have shown that the use of different separation methodologies can lead to quite different outcomes regarding GW climatologies, even after removing the possible presence of planetary waves. Then, either due to the imperfect nature of the separation methodologies or due to the presence of other possible variable factors that are not waves (may be phenomena not contemplated in the separation procedure like for

example the presence of transient effects triggered by instabilities), the calculated activity may include GW but also other features. Moreover, GW are intermittent (Alexander and Barnet, 2007). There may be then an ambient activity (corresponding to the variabilities not related to GW) which is a kind of ensemble of diverse typical mesoscale structures which are present whether there are or not GW and whose intensity may depend on the region and season being analyzed. In the simple separation procedure into two components this fact inevitably contaminates the GW part. In this first approach we assume without further support that the ambient activity is steady in the analyzed region over the four seasons. Future work on this issue may eventually relax this condition.

Another issue of the energy distribution of GW in a given region and season is the skewed shape (Baumgaertner and McDonald, 2007; Alexander et al., 2010, 2015, e.g.,). This property led these works to suggest that the median could be a more representative parameter than the mean to characterize the wave activity. The sharp drop to the left of the peak of the energy distribution (towards zero energy in Fig. 2) has not been given up to now an interpretation in terms of basic physical concepts or in terms of the observational window or in terms of errors of the sounding technique. Is it a consequence of true GW characteristics or is it caused by limitations of the observational method? Here we give a possible perspective. We suggest that this behavior may not reflect a true distribution issue but could be ascribed to a precision limit of the GPS RO method, which could wipe out a possible increasing behavior towards the lowest energy values. Although different satellite remote sensing techniques might be detecting different portions of the GW spectrum, a similar effect might be observed as they typically have the same order of magnitude precision limits. We make a rough estimation to substantiate our argument. RO T profiles may be considered precise to roughly 0.5 K (Hajj, 2004; Kuo, 2005). An integer number of sinusoidal oscillations with $T' = 0.5$ K in a typical background in the stratosphere where $T_b = 220$ K and $N = 0.02\ s^{-1}$ lead in Eq. (1) to $E_p = 0.3$ J/kg. Any energy results close to and smaller than this uncertainty limit should be considered dubious. Then, several true low energy cases may usually become decimated when observed by GPS RO and may be then artificially projected as higher energies events. To recover the low energy cases that were apparently lost, we conjecture here a "true" exponential-like distribution that in general seems to join nicely the behavior of the unharmed portion and we try to demonstrate its feasibility. The energy distribution maxima were found below between 0.3 and 0.4 J/kg in 12 of our 16 categories (we recall however that the mode and other statistical characteristics of the energy distributions may depend in detail on the filter used, the minimum and maximum wavelength cutoffs and the vertical integration column used in each study according to (Luna et al., 2013)). Then, from our above calculations the E_p values may be considered dubious from around the mode to the left of the distribution. If we do not make any appropriate correction, then all the corresponding statistical measures obtained from the observed

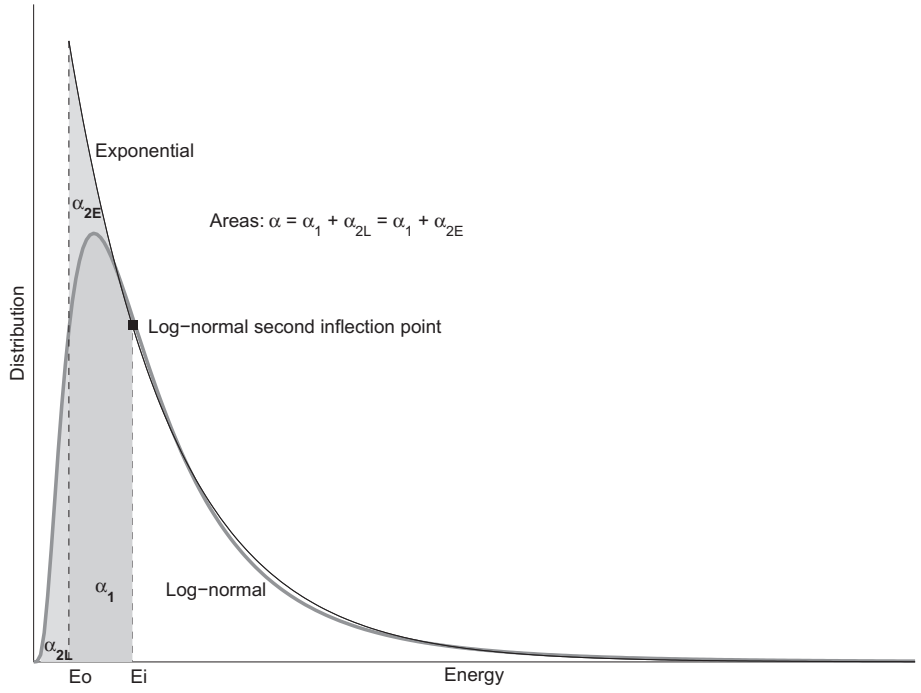

Fig. 2. The log-normal and exponential functions as different alternatives to represent the GW energy distribution observed from GPS RO. The log-normal curve has two inflection points: one at a lower and one at a higher value than the mode, the latter being called here the second inflection point. The vertical axis has no units as it represents a probability density.

distribution may be flawed. As a final consideration, a normal distribution for E_p can be straightforwardly discarded, as in some of the 16 categories the standard deviation was found to be larger than the mean value (using a Gaussian model would imply that more than 16% of the events would have un-physical negative energies).

3. Results

We now consider for the 16 categories a representative parameter for the GW activity contained in the atmosphere and its associated uncertainty according to three diverse schemes for interpreting the observed energy distribution: (1) in some works the energy mean is calculated without any assumption on the energy distribution. (2) In other cases the skewed shape becomes interpreted in terms of a log-normal (Baumgaertner and McDonald, 2007) or a Gamma (Alexander et al., 2015) distribution. The former option will be used here as it seems to have a slightly better performance and the corresponding median will be calculated. (3) We suggest a different perspective of the observed skewed distribution: it would mask due to GPS RO precision artifacts a "true" rising distribution towards the lowest energies. Then, the curve to the left of the second inflection point (rather than the mode) of the log-normal shape would be a consequence of an attenuation in the detection of GW due to precision issues. This part of the curve should therefore not be used for the calculation of representative values of the distribution. We then conjecture that an exponential curve could be a better representation of the observable energy distribution, which to the left of the second inflection point at E_i would follow from an extrapolation up to some threshold energy E_o (see Fig. 2). In an exponential distribution starting at 0 the mean is the maximum likelihood estimate of the lifetime factor λ characterizing it. The standard deviation of the sample is also λ. As we postulate that we do not have reliable information to the left of the second inflection point we will ignore those data, so we look now for the maximum likelihood estimate of the lifetime factor for a truncated exponential (available energy data do not belong to the interval between 0 and ∞, but to the range from the log-normal second inflection point value to ∞). This problem has already been addressed by Fraile and García-Ortega (2005), showing that λ must then be calculated as the mean (with unreliable data already excluded) minus the truncating value.

In Table 1 we show the fitted values for the relevant parameters of the three diverse representations. In the exponential curve we consider the shifted mean $\lambda + E_o$, as the distribution is horizontally shifted by E_o (see Fig. 2 and Appendix A). The uncertainties associated to the 90% confidence intervals have been obtained. Notwithstanding the lack of a distribution in the first scheme, the central limit theorem implies that the mean follows a Gaussian distribution. In the remaining two representations the uncertainties can only be obtained by approximations (Parkin and Robinson, 1993; Ross, 2009, e.g.,) and are not symmetric in some cases. The amounts of RO retrievals in each category are also shown (recall that a subset of the soundings was put away for the exponential fit) in order to contextualize the statistical strength of the results. Alexander et al. (2015) have shown that the E_p distributions obtained from GPS RO data could be contaminated by the presence of some spurious large GW activity cases located in the distribution tail. They are possible artifacts generated by initialization problems in some retrievals that were not ruled out by the quality control process. In order to consider this issue in the exponential distribution, we also need to include an upper threshold. The calculation of λ for this doubly truncated exponential has also been contemplated by Fraile and García-Ortega (2005). In our case the upper threshold is typically 4 J/kg (Alexander et al., 2015), which is much larger than the usual values

Table 1
The values calculated for the representative parameters of three diverse schemes to interpret the RO measurements as indicators of GW E_p and their confidence intervals to a 90% level. The amount of RO retrievals used in the models is also shown. Data have been classified in terms of season, favorable or unfavorable LOS and location to the West or East of the Andes Range. Energies are given in J/kg.

Season	FW	FE	UW	UE
Non-parametric approach: sample mean, [confidence limits], amount of RO				
DJF	0.77, [0.71 0.83], 212	0.72, [0.67 0.76], 178	0.65, [0.60 0.70], 73	0.76, [0.69 0.83], 91
MAM	0.63, [0.59 0.66], 240	0.68, [0.61 0.75], 184	0.54, [0.49 0.59], 117	0.63, [0.56 0.69], 84
JJA	0.72, [0.65 0.79], 193	0.98, [0.83 1.12], 168	0.70, [0.59 0.80], 65	0.84, [0.70 0.98], 88
SON	0.53, [0.48 0.58], 173	0.61, [0.56 0.67], 166	0.57, [0.49 0.64], 77	0.70, [0.57 0.83], 67
Log-normal distribution: median, [confidence limits], amount of RO				
DJF	0.68, [0.64 0.72], 212	0.65, [0.61 0.68], 178	0.59, [0.54 0.65], 73	0.68, [0.62 0.74], 91
MAM	0.56, [0.53 0.59], 240	0.57, [0.53 0.61], 184	0.47, [0.43 0.51], 117	0.55, [0.50 0.60], 84
JJA	0.55, [0.50 0.60], 193	0.63, [0.56 0.70], 168	0.57, [0.50 0.65], 65	0.60, [0.52 0.69], 88
SON	0.44, [0.41 0.47], 173	0.49, [0.45 0.54], 166	0.46, [0.40 0.52], 77	0.53, [0.45 0.61], 67
Two-parameter exponential distribution: mean, [confidence limits], amount of RO				
DJF	0.80, [0.79 0.80], 85	0.75, [0.75 0.75], 67	0.69, [0.69 0.69], 31	0.80, [0.79 0.80], 36
MAM	0.66, [0.66 0.66], 83	0.70, [0.69 0.71], 71	0.56, [0.56 0.57], 53	0.66, [0.65 0.67], 30
JJA	0.72, [0.69 0.76], 105	1.00, [0.92 1.10], 94	0.70, [0.68 0.74], 33	0.83, [0.77 0.92], 50
SON	0.55, [0.53 0.56], 77	0.62, [0.60 0.64], 82	0.57, [0.55 0.61], 38	0.67, [0.64 0.74], 41

of the lower threshold E_o and the new expression of λ then reduces to the one already used above. However, different λ values and confidence intervals may now be obtained as $E_p > 4$ J/kg cases are excluded in the new calculations. Only 3 from the 16 cases for the exponential distribution in Table 1 underwent modifications of the values, which were small and did not modify the essence of the results. These recalculations are therefore not included.

The effect of Andes is very clear when comparing each pair of East and West E_p representations, as the values are always larger on the former side with only one exception in the three distribution schemes: during summer in the favorable cases. Our results show that the seasonal maximum of E_p on the Eastern side for the favorable cases during winter has statistical significance at the 90% level in schemes (1) and (3). However, the difference of GW activity indicators between favorable and unfavorable LOS is significant only for (3). During summer there are higher E_p values with respect to spring and autumn, which could be attributed to GW generation by deep convection. In some cases differences are statistically significant at the 90% level. This type of waves may not have a preferential orientation and may not exhibit a lack of displacement like MW and could therefore produce effects on both LOS groups and to the East and West of the Andes Range. The results of Table 1 have been illustrated in Fig. 3. It can there also be clearly seen that the representative E_p values for the non-parametric case and for the exponential distribution are quite similar under given zone (West or East), season and LOS classification (favorable or unfavorable), but in general the uncertainty for the latter scheme is much lower.

In general, we may conclude that with our digital filter and definitions of wavelength cutoffs and vertical integration column there is a permanent ambient energy noise level about 0.5 J/kg and in the highest season up to another 0.5 J/kg according to intermittency and intensity levels of MW becomes added. A smaller effect is to be expected from deep convection during summer. These estimations probably differ from real GW energy values as GPS RO are expected to underestimate GW amplitudes and see just a portion of the full spectrum (Alexander et al., 2008), but there are no optimal observational methods regrading this kind of drawbacks.

We introduced here a new model to interpret GW energy distributions in trying to correct what we consider an artifact at the lowest values due to the precision limits of the technique. If the suggested procedure is correct, then it should improve the calculation of statistical measures

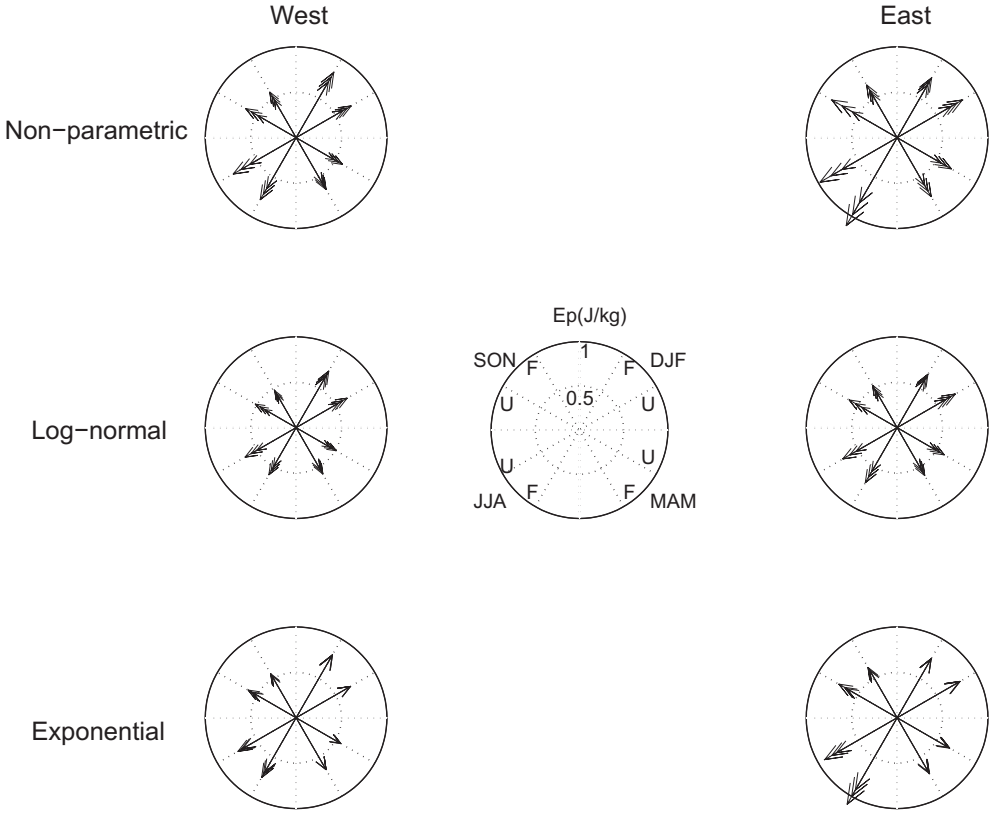

Fig. 3. The values calculated for the representative parameters of the three diverse schemes, which are indicators of GW E_p to the West and to the East of Andes. The three consecutive arrow tips in each radius (in some cases they cannot be distinguished) represent each value and the 90% level confidence interval. The polar representation in the middle of the figure shows how to interpret every individual plot: each quadrant corresponds to a season, each line direction is related to a LOS classification of the retrievals (F look here rather vertical-like and U more horizontal-like), whereas the radius of the full circle is equivalent to $E_p = 1$ J/kg.

like the mean, regardless of the source of the GW (topography, convection, instabilities, etc.). In this work we are interested in applying our procedure in a region dominated by MW in winter and convection in summer. On the other hand, the preference of COSMIC for LOS aligned about the North–South direction can be clearly appreciated in the fact that the number of cases within angles ±30° is in every season and in both regions typically more than twofold as compared with the number of soundings within 45–135° (notice that the angular interval in the latter case is 50% larger). This means that due to this characteristic COSMIC will by its own tend to highlight the winter energy increase by topographic sources in this zone as compared to other existing or possible future GPS RO configurations.

Besides the above mentioned difficulties in the separation of background and GW in the measured profiles, other factors that may disrupt this simple scheme should be at least noted. Zhang et al. (2012) and Zhang et al. (2013) have analyzed radiosonde observations of GW at mid-latitudes in the Northern Hemisphere which include horizontal wind. They showed the possible significant impact of the variation of background dynamics and thermal structures on GW properties. At the same time they also revealed the potential of GW to produce important effects on modifying the background atmosphere.

We assessed the degree of favorable conditions for MW generation according to season by calculating for the latitude range 36–29S and longitude 70 W the mean zonal velocity at about the height of the highest mountains (500 mb ~ 5 km height) and the variability by the standard deviation (see Table 2). The data used were monthly means between years 2007 and 2012 from NCEP (National Center for Environmental Prediction) reanalysis. Winter and spring are clearly optimal seasons regarding the intense zonal wind in the troposphere as a source of topographic GW. Zonal wind speeds at stratospheric heights may typically reach in the analyzed region null values at heights about 50 mb (~ 22 km height). This may then become a critical level for MW, which are usually expected to be stationary. According to our results only during summer would then MW become probably filtered at stratospheric heights (see Table 2). This does not apply to other sources like convection, because those waves are not expected to be steady.

Table 2
Mean zonal wind and standard deviation at 500 mb (U_{500} and σ_{U500}) and mean zonal wind and standard deviation at 50 mb (U_{50} and σ_{U50}). The data used were monthly NCEP reanalysis means above the studied region between years 2007 and 2012 and were classified in terms of season.

Season	U_{500} (m/s), σ_{U500} (m/s)	U_{50} (m/s), σ_{U50} (m/s)
DJF	8.4, 2.9	−1.3, 2.5
MAM	9.7, 2.0	5.2, 4.5
JJA	15.5, 2.0	12.3, 2.9
SON	13.8, 3.0	5.5, 3.9

4. Conclusions

We conclude that the use of a given mathematical representation of the energy distribution of GW or the use of data from a mission with given preferential characteristics may have confounding consequences or may blur some aspects highlighted by others. Interpretations are distribution model and mission dependent besides the capability of GPS RO to distinguish the waves. We suggest that a reinterpretation of the E_p distribution observed by GPS RO at the lowest values may improve the possible detection of GW activity. In our analysis it produces observable results for MW, as it highlights the expected E_p difference between the East and West sectors in winter. Other effects observable by GPS RO for the remaining seasons and/or sources are a priori not so clear in the region that we studied, so we cannot check whether there have been improvements in those other cases. However, the E_p distribution model that we introduced should in general improve the detection of GW of any source. These conclusions may apply but should not be straightforwardly extended to data from other limb sounders, as the specific characteristics of each measurement technique must be considered in each case. The GPS RO properties and how they influence the detection of GW have been given e.g. by Alexander et al. (2008). Finally, we also consider that the observed E_p distribution obtained from any measurement technique should be defined as the contributions from waves but also from unspecific variable ambient phenomena, because the latter component is usually ignored.

Acknowledgements

Manuscript prepared under grant CONICET PIP 11220090100649 and ANPCyT 2013-1097. P. Alexander, A. de la Torre, R. Hierro and P. Llamedo are members of CONICET. GPS RO data were downloaded from CDAAC at cosmic-io.cosmic.ucar.edu/cdaac/index.html and NCEP reanalysis downloaded from www.esrl.noaa.gov/psd/data/timeseries.

Appendix A. The truncated exponential distribution parameters

Following Fraile and García-Ortega (2005) for a left truncated exponential fit (no information is known to the left of some given value E_i)

$$\lambda = \overline{E}|_{E \geqslant E_i} - E_i \tag{A.1}$$

where $\overline{E}|_{E \geqslant E_i}$ is the average over all the measured energies above E_i (here it is the energy value at the second log-normal inflection point). If the energy results for a set of GPS RO retrievals are interpreted as the outcome of a log-normal distribution, then in terms of the mean and standard deviation of the associated normal distribution μ and σ (Maccone et al., 2012)

$$E_i = e^{\mu-\frac{3}{2}\sigma^2+\frac{\sigma}{2}\sqrt{4+\sigma^2}} \quad (A.2)$$

and λ in Eq. (A.1) can then be calculated.

We should not disclose the possibility that there is some threshold minimum energy value for the exponential distribution (either waves in the very small energy range are not created at all or they could be eliminated by some mechanism like dissipation or instability). Moreover, from Fig. 2 we can see that if the log-normal and exponential distributions nearly coincide to the right of the second inflection point, then the areas under both curves to the left must nearly be equal and the exponential distribution is likely to have some threshold value above zero. We therefore postulate a two-parameter (λ and threshold energy value E_o) exponential distribution (Kececioglu, 2002, e.g.,). Although Eq. (A.1) from Fraile and García-Ortega (2005) has been derived for the one-parameter exponential distribution ($E_o = 0$), it is easily extendable to the two-parameter distribution by a simple horizontal shift. E_o can be determined from two properties related to the second inflection point of the log-normal distribution, which in turn depend on the two parameters of the associated normal distribution. We first recall that for the two-parameter exponential distribution function

$$\int_{E_o}^{\infty} \frac{1}{\lambda} e^{-\left(\frac{E-E_o}{\lambda}\right)} dE = 1 \quad (A.3)$$

The exponential distribution must resemble the log-normal curve to the right of the second inflection point. Then the areas under both curves between E_i and ∞ must be equal. The same applies then to both areas to the left of E_i, which we call α

$$\int_{E_o}^{E_i} \frac{1}{\lambda} e^{-\left(\frac{E-E_o}{\lambda}\right)} dE = \alpha \quad (A.4)$$

which leads to

$$E_o = E_i + \lambda \ln(1-\alpha) \quad (A.5)$$

According to Maccone et al. (2012) at the second inflection point of the log-normal

$$\alpha = \frac{1}{2} + \frac{\operatorname{erf}\left(\frac{\sqrt{4+\sigma^2}-3\sigma}{2^{\frac{3}{2}}}\right)}{2} \quad (A.6)$$

In brief, we first look for the two parameters of the associated Gaussian distribution, and through Eqs. (A.2) and (A.6) are then able to find E_i and α, which are related to the second inflection point of the log-normal distribution. Then finally λ and thereafter E_o of the two-parameter exponential distribution can be determined after Eqs. (A.1) and (A.5). Notice that it is possible to obtain E_o, not through a statistical estimator, but after an area preserving constraint (the imposed similarity of the log-normal and exponential curves to the right of E_i, where data are supposedly not distorted). The calculated value of E_o is not only an estimation of the order of magnitude of the threshold energy in each case, but also a rough check of consistency of the two-parameter exponential model (it must be >0). We calculated the two-parameter exponential mean $\lambda + E_o$ uncertainty (Table 1) only due to the λ confidence interval and notice from Eq. (A.5) that the effect introduced becomes attenuated by the factor $1 + \ln(1-\alpha)$ (the second term is typically around -0.6).

It is interesting to notice from Eqs. (A.2) and (A.6) that E_i can be smaller or larger than the median e^{μ} and so α can be smaller or larger than 0.5 (the argument of the function erf can be positive or negative). We also notice that if the energy threshold E_o was considered to be 0 instead of being calculated, then the distribution function would be the same curve shifted horizontally to the left by E_o. As the condition of Eq. (A.5) would not be set, then to the right of E_i the exponential fit would likely resemble the shape but possibly not the log-normal curve values, which are presumed to be the "true" ones.

References

Alexander, M.J., Barnet, C., 2007. Using satellite observations to constrain parameterizations of gravity wave effects for global models. J. Atmos. Sci. 64, 16521665. http://dx.doi.org/10.1175/JAS3897.1.

Alexander, P., de la Torre, A., Llamedo, P., 2008. Interpretation of gravity wave signatures in GPS radio occultations. J. Geophys. Res. 113, D16117. http://dx.doi.org/10.1029/2007JD009390.

Alexander, P. et al., 2010. A gravity waves study close to the Andes mountains in Patagonia and Antarctica with GPS radio occultation observations. Ann. Geophys. 28, 587–595.

Alexander, P. et al., 2011. A method to improve the determination of wave perturbations close to the tropopause by using a digital filter. Atmos. Meas. Tech. 4, 1777–1784.

Alexander, P., Luna, D., de la Torre, A., Schmidt, T., 2015. Distribution functions and statistical parameters that may be used to characterize limb sounders gravity wave climatologies in the stratosphere. Adv. Space Res. 56, 619–633. http://dx.doi.org/10.1016/j.asr.2015.05.007.

Alexander, S.P., Klekociuk, A.R., Tsuda, T., 2009. Gravity wave and orographic wave activity observed around the Antarctic and Arctic stratospheric vortices by the COSMIC GPS-RO satellite constellation. J. Geophys. Res. 114, D17103. http://dx.doi.org/10.1029/2009JD011851.

Baines, P.G., 1995. Topographic Effects in Stratified Fluids. Cambridge Univ. Press, New York, 482pp.

Baumgaertner, A., McDonald, A., 2007. A gravity wave climatology for Antarctica compiled from Challenging Minisatellite Payload/Global Positioning System (CHAMP/GPS) radio occultations. J. Geophys. Res. 112, D05103.

de la Torre, A., Alexander, P., 2005. Gravity waves above Andes detected from GPS radio occultation temperature profiles: Mountain forcing?. Geophys. Res. Lett. 32 L17815. http://dx.doi.org/10.1029/2005GL022959.

de la Torre, A., Alexander, P., Llamedo, P., Menéndez, C., Schmidt, T., Wickert, J., 2006. Gravity waves above the Andes detected from GPS radio occultation temperature profiles: jet mechanism? Geophys. Res. Lett. 33, L24810. http://dx.doi.org/10.1029/2006GL027343.

Fraile, R., García-Ortega, E., 2005. Fitting an exponential distribution. J. Appl. Meteorol. 44, 1620–1625.

Hajj, G.A. et al., 2004. CHAMP and SAC-C atmospheric occultation results and intercomparisons. J. Geophys. Res. 109, D06109.

Hindley, N.P., Wright, C.J., Smith, N.D., Mitchell, N.J., 2015. The southern stratospheric gravity wave hot spot: individual waves and their momentum fluxes measured by COSMIC GPS-RO. Atmos. Chem. Phys. 15, 7797–7818.

Jin, S.G., Feng, G.P., Gleason, S., 2011. Remote sensing using GNSS signals: current status and future directions. Adv. Space Res. 47, 1645–1653. http://dx.doi.org/10.1016/j.asr.2011.01.036.

John, S.R., Kumar, K.K., 2013. A discussion on the methods of extracting gravity wave perturbations from space-based measurements. Geophys. Res. Lett. 40, 24062410. http://dx.doi.org/10.1002/grl.50451.

Kececioglu, Dimitri B., Reliability Engineering Handbook, DEStech Publications, Lancaster (PA), vol. 1, 2002, 720 pp.

Kuo, Y.-H. et al., 2005. Comparison of GPS radio occultation soundings with radiosondes. Geophys. Res. Lett. 32, L05817. http://dx.doi.org/10.1029/2004GL021443.

Kursinski, E. et al., 1997. Observing earth's atmosphere with radio occultation measurements using the global positioning system. J. Geophys. Res. 102, 23429–23465.

Llamedo, P. et al., 2009. A gravity wave analysis near to the Andes Range from GPS radio occultation data and mesoscale numerical simulations: two case studies. Adv. Space Res. 44, 494500. http://dx.doi.org/10.1016/j.asr.2009.04.023.

Luna, D., Alexander, P., de la Torre, A., 2013. Evaluation of uncertainty in gravity wave potential energy calculations through GPS radio occultation measurements. Adv. Space Res. 52, 879–882. http://dx.doi.org/10.1016/j.asr.2013.05.015.

Maccone, C., 2012. Mathematical SETI: Statistics, Signal Processing, Space Missions. Springer, Heidelberg, 724pp.

Marquardt, C., Healy, S., 2005. Measurement noise and stratospheric gravity wave characteristics obtained from GPS occultation data. J. Meteorol. Soc. Jpn. 83, 417–428.

McDonald, A.J., Hertzog, A., 2008. Comparison of stratospheric measurements made by CHAMP radio occultation and Strateole/Vorcore in situ data. Geophys. Res. Lett. 35, L11805. http://dx.doi.org/10.1029/2008GL033338.

Parkin, T.B., Robinson, J.A., 1993. Statistical evaluation of median estimators for lognormally distributed variables. Soil Sci. Soc. Am. J. 57, 317–323.

Ross, S.M., 2009. Introduction to Probability and Statistics for Engineers and Scientists, fourth ed. Academic Press, London, 680pp.

Sacha, P., Foelsche, U., Pisoft, P., 2014. Analysis of internal gravity waves with GPS RO density profiles. Atmos. Meas. Tech. 7, 41234132.

Wilson, R., Chanin, M.L., Hauchecarne, A., 1991. Gravity waves in the middle atmosphere observed by Rayleigh lidar 1. Case studies. J. Geophys. Res. 96, 5153–5167.

Wu, D.L. et al., 2006. Remote sounding of atmospheric gravity waves with satellite limb and nadir techniques. Adv. Space Res. 37, 2269–2277.

Zhang, S.D., Yi, F., Huang, C.M., Huang, K.M., 2012. High vertical resolution analyses of gravity waves and turbulence at a midlatitude station. J. Geophys. Res. 117, D02103. http://dx.doi.org/10.1029/2011JD016587.

Zhang, S.D., Yi, F., Huang, C.M., Huang, K.M., Gan, Q., Zhang, Y.H., Gong, Y., 2013. Latitudinal and altitudinal variability of lower atmospheric inertial gravity waves revealed by U.S. radiosonde data. J. Geophys. Res. 118, 7750–7764. http://dx.doi.org/10.1002/jgrd.50623.